https://doi.org/10.5194/wes-2023-167
Preprint. Discussion started: 15 January 2024

eawe european academy of wind energy
Open Access WIND ENERGY SCIENCE DISCUSSIONS

Non-proportionality analysis of multiaxial fatigue stress histories in trailing edge adhesive joints of wind turbine rotor blades

Claudio Balzani[1] and Pablo Noever Castelos[1]

[1]Leibniz University Hannover, Institute for Wind Energy Systems, Appelstr. 9A, 30167 Hannover, Germany

Correspondence: Claudio Balzani (research@iwes.uni-hannover.de)

Abstract. Wind turbine rotor blades are exposed to complex multiaxial stress states due to the aero-(hydro-)servo-elastic behaviour of the turbine. The dynamic response of rotor blades can result in non-proportional stress histories in the adhesive joints. These are not properly considered in current design guidelines and standards. However, knowledge about the degree of non-proportionality is crucial for choosing an appropriate fatigue analysis framework.

This paper investigates the degree of non-proportionality of three-dimensional stress histories in trailing edge adhesive joints of wind turbine rotor blades. For the quantification of non-proportionality, the concept of so-called non-proportionality factors is utilized. Existing approaches show weaknesses for the application to adhesives. Hence, a novel non-proportionality factor is introduced in this work that combines two formulations from literature. After a concise verification, it is applied to analyze the trailing edge adhesive joints of three different blade designs in the framework of a numerical comparative study.

The results do not reveal any correlation between the degree of non-proportionality and the blade size. General conclusions are hard to draw, as the blade response does not only depend on the turbine size, but also on the blade design philosophy. However, each blade shows significant degrees of non-proportionality that should not be neglected in fatigue damage analyses.

1 Introduction

During a wind turbine's lifetime, rotor blades and their adhesive joints are subjected to multiaxial stress states. According to current design guidelines for wind turbine rotor blades (e.g., DNV GL, 2015), fatigue analyses of adhesive joints have to take into account these multiaxial stress states. However, these regulations lack of clear descriptions of associated analysis procedures. Picking up longterm research goals formulated by van Kuik et al. (2016); van Kuik and Peinke (2016), the question arises if failure of adhesive joints exposed to multiaxial fatigue loads can be well predicted. A thorough understanding of the nature of stress states in the adhesives throughout their lifetime is inevitable for choosing (or developing) an appropriate fatigue analysis framework and for designing validation test methods.

Fatigue analyses may follow global stress-strength relationships, see e. g. von Mises (1913); Schleicher (1926); Drucker and Prager (1952); Stassi-D'Alia (1967); Raghava et al. (1973); Christensen (2004) or similar approaches. These take into account the complete three-dimensional stress tensor and have already been applied to rotor blade adhesives (Noever Castelos and Balzani, 2016a; Antoniou et al., 2018; Eder et al., 2020). This approach translates the stress tensor to the scalar-valued global equivalent stress, which is easy to handle in a classical rainflow counting scheme (Endo et al., 1974; Downing and Socie,

https://doi.org/10.5194/wes-2023-167
Preprint. Discussion started: 15 January 2024

eawe european academy of wind energy
Open Access WIND ENERGY SCIENCE DISCUSSIONS

1982; Rychlik, 1987; Lee and Tjhung, 2012). However, the transition from an engineering stress space to an equivalent stress space must thoroughly consider potential tension-compression asymmetries (which are present in epoxy-based adhesives), and the method is only valid for proportional stress histories, see e. g. Kuhn et al. (2023). In this case, the major principal stress direction is not changing with time, but the amplitude may vary (Stephens et al., 2001).

However, the loads acting on rotor blades are strongly dynamic (Söker, 2013; Liu et al., 2017) and non-linear (Manolas et al., 2015; Noever Castelos and Balzani, 2016b). E.g., lead-lag bending (also known as edgewise bending), which is governed by the rotor blades' inertia, is mostly deterministic and harmonic with an excitation frequency of the rotor rotation speed and multiples thereof. On the other hand, fore-aft bending (also called flapwise bending) is triggered by aerodynamic forces. These are more stochastic in the time domain, due to the turbulent wind inflow (White and Musial, 2004). Speaking more clearly, the normal stress in spanwise direction is dominant in trailing edge adhesive joints, and is mainly caused by lead-lag bending (Noever Castelos and Balzani, 2016a). The fore-aft bending contributes to the normal stress to a minor extent due to a smaller offset from the related principal bending axis (Bak et al., 2013), but is, besides torsion, predominantly responsible for shear stresses in the trailing edge adhesive joint. Since the lead-leg and the fore-aft loads are generally not in phase, the share of each stress component in the three-dimensional stress tensor will change in time. Consequently, the orientation of the major principal stress changes as well, which, by definition (e.g., Socie and Marquis, 2000), results in non-proportional stress time series. These cannot be captured by global equivalent stress approaches (Fatemi and Shamsaei, 2011; Kuhn et al., 2023).

A physically more meaningful way is to apply the critical plane approach (Socie and Marquis, 2000; de Castro and Meggiolaro, 2016; Deng et al., 2022, 2023). Therein, the damage calculation is restricted to the plane on which a physical crack will appear, which is called the critical plane. Such concepts evaluate local equivalent stress functions that are formulated on the critical plane and take into account the normal stress perpendicular and the two shear stresses (or the resulting shear stress) parallel to such plane. However, the orientation of the critical plane may change with time, which is linked to the orientation change of the first principal stress (Anes et al., 2014). It is thus not known *a priori* in non-proportional stress histories and needs to be a result of the fatigue analysis. A computationally efficient method for the determination of the critical plane orientation was proposed by Wentingmann et al. (2018).

The choice of an appropriate fatigue analysis concept depends on the degree of non-proportionality. It is thus important to gain deep knowledge of the characteristics of stress histories in rotor blade adhesive joints and to quantify the degree of non-proportionality in the stress histories, which is the focus of this paper. The concept of non-proportionality factors is employed. Some of the formulations available in literature are briefly reviewed in section 2. As all of them show weeknesses for adhesive joints, a novel non-proportionality factor is proposed that combines two existing formulations. The new non-proportionality factor is verified using numerical examples from literature. The stress histories in trailing edge adhesive joints of three different rotor blade designs are subsequently analyzed: (i) the 86 m DTU 10 MW Reference Wind Turbine Blade (Bak et al., 2013), (ii) the 80 m IWES IWT-7.5-164 Reference Wind Turbine Blade (Sevinc et al., 2016) from the *Smart Blades* project (Teßmer et al., 2016), and (iii) the 20 m Demonstration Blade (Bätge, 2016) from the *SmartBlades2* project (called *SB2-DemoBlade* in the following). The latter blade has a pre-sweep in the rotor area for introducing a geometrical bend-twist coupling, which is a particularity worth mentioning. The blades were chosen as the first two are similar in size and the third is significantly

https://doi.org/10.5194/wes-2023-167
Preprint. Discussion started: 15 January 2024

eawe european academy of wind energy
Open Access WIND ENERGY SCIENCE DISCUSSIONS

smaller. In this way we can compare different blade sizes while taking into account different design philosophies for the large blades. The degrees of non-proportionality in all three blades are compared in terms of a numerical comparative study using the proposed non-proportionality factor. The results are thoroughly discussed and give an indication for the choice of appropriate fatigue analysis concepts for the design of next generation rotor blades.

2 Quantification of non-proportionality in multiaxial stress histories

Socie and Marquis (2000) briefly present a selection of approaches to calculate a so-called non-proportionality factor f_{NP}. These have in common that a data point is plotted in the stress domain for each time instance of the stress time series. The conglomeration of all these points forms a body in the six-dimensional stress space[1]. The first approach considers f_{NP} as the aspect ratio of a minimum size convex surface surrounding this body, which would be an ellipsis in a two-dimensional case. This concept is visualised for three different artificial 2D cases in Figure 1, where the shear stress τ_{xy} is combined with the normal stress σ_x.

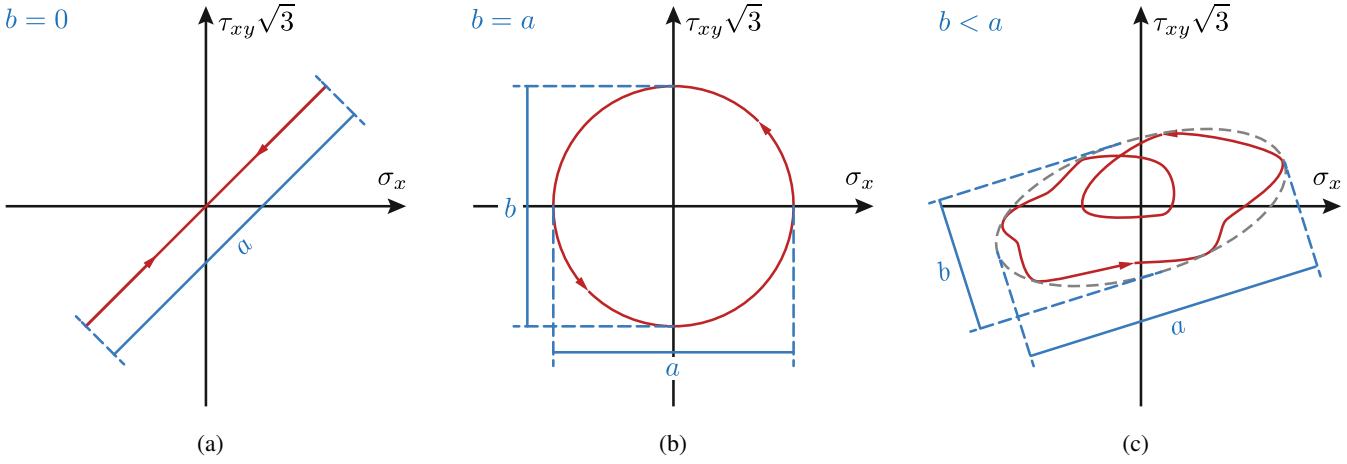

Figure 1. Minimum size convex hull surrounding the body spanned by the data points of stress instances in the stress time series in the two-dimensional case (reproduced from Socie and Marquis (2000)): (a) proportional stress time series with $f_{NP} = \frac{b}{a} = 0$ (expressed by a straight line, i. e. $b = 0$); (b) stress time series with 90° phase shift and $f_{NP} = \frac{b}{a} = 1$ (as $a = b$); (c) arbitrary time series with $0 < f_{NP} < 1$ for $a > b$.

This convex hull method is easy to apply in the 2D stress space. However, it becomes more complicated with increasing dimension, as one needs to compute ellipsoids in the 3D stress space or hyper-ellipsoids in the general case, as Zouain et al. (2006) discuss in detail. Besides, the non-physical and rather geometric nature of this method is linked with a loss of information on the cyclicity of the stress time series due to the generalizing hull, and can lead to poor predictions of f_{NP} depending on

[1]The stress space is six-dimensional only if the complete stress tensor is included. It is e. g. reduced to three dimensions if only the normal stresses are considered.

https://doi.org/10.5194/wes-2023-167
Preprint. Discussion started: 15 January 2024

eawe european academy of wind energy
Open Access WIND ENERGY SCIENCE DISCUSSIONS

the load path complexity (Meggiolaro and de Castro, 2012). Kanazawa et al. (1979) presented a different approach estimating f_{NP} by means of a rotation factor, which is defined by

$$f_{NP} = \frac{\text{Shear strain } 45^\circ \text{ to maximum shear strain range}}{\text{Maximum shear straing range}}. \tag{1}$$

This factor represents the ellipticity of the load path in the τ_{xy} vs. σ_x biaxial stress space and depends on both the phase angle and the amplitude (Socie and Marquis, 2000). Following a similar idea, Itoh et al. (1995) integrated the product of the highest principal strain of the load path, ε_1, and its angular deviation to the maximum value of ε_1, ξ, over the related time period T according to

$$f_{NP} = \frac{\pi}{2T\varepsilon_{1,\max}} \int_0^T \varepsilon_1(t)\, |\sin(\xi(t))|\, \mathrm{d}t\,. \tag{2}$$

Herein, $\varepsilon_{1,max}$ denotes the maximum value of ε_1 in the time series, i. e., $\varepsilon_{1,max} = \max\{\varepsilon_1(t)\}$, $|(\bullet)|$ is the norm of $(\bullet)$, and t is the time. This expression for 2D load paths was later extended to a 3D expression in Itoh et al. (2013). However, it is still not applicable for the general 6D case.

A different formulation was introduced by Bishop (2000) using an analogy to mass moments of inertia. Using Voigt notation, he represented the symmetric second order stress tensor, the metrics of which defined by a 3×3 matrix, by a six-dimensional vector $\boldsymbol{\sigma}_M \in \mathbb{R}^6$ following

$$\boldsymbol{\sigma}_{3\times3} = \begin{pmatrix} \sigma_{11} & \sigma_{12} & \sigma_{13} \\ \sigma_{21} & \sigma_{22} & \sigma_{23} \\ \sigma_{31} & \sigma_{32} & \sigma_{33} \end{pmatrix} \quad \Rightarrow \quad \boldsymbol{\sigma}_M = \left(\sigma_{11}, \sigma_{22}, \sigma_{33}, \sqrt{2}\sigma_{12}, \sqrt{2}\sigma_{13}, \sqrt{2}\sigma_{23}\right)^{\mathrm{T}}. \tag{3}$$

The full matrix of mass moments of inertia of the body spanned by the stress instances along the time series in the full six-dimensional stress space, which is denoted by $\boldsymbol{I} \in \mathbb{R}^6$, can be computed according to

$$\boldsymbol{I} = \oint_\Sigma (\boldsymbol{\sigma}_M - \overline{\boldsymbol{\sigma}})(\boldsymbol{\sigma}_M - \overline{\boldsymbol{\sigma}})^T\, |\mathrm{d}\boldsymbol{\sigma}|\,. \tag{4}$$

Herein, the moment of inertia matrix is calculated with respect to the mean stress $\overline{\boldsymbol{\sigma}}$, which is determined by the expression

$$\overline{\boldsymbol{\sigma}} = \frac{1}{L} \oint_\Sigma \boldsymbol{\sigma}_M\, |\mathrm{d}\boldsymbol{\sigma}_M|\,, \quad \text{with} \quad L = \oint_\Sigma |\mathrm{d}\boldsymbol{\sigma}|\,. \tag{5}$$

Provided that $|\mathrm{d}\boldsymbol{\sigma}|$ represents the Euclidean distance between two time steps, L reflects the complete Euclidean arc length of the stress path Σ. Calculation of the n eigenvalues λ_i of the mass moment of inertia matrix $\boldsymbol{I}$ and sorting them in decreasing order, i. e., $\lambda_1 > \lambda_2 > ... > \lambda_n$, yields the non-proportionality factor according to Bishop (2000) defined by

$$f_{NP} = \sqrt{\frac{\lambda_2}{\lambda_1}}. \tag{6}$$

Meggiolaro et al. (2016) analysed this expression and concluded the following: (i) Equation (6) is formulated in the stress space

https://doi.org/10.5194/wes-2023-167
Preprint. Discussion started: 15 January 2024

eawe european academy of wind energy
Open Access WIND ENERGY SCIENCE DISCUSSIONS

instead of a more appropiate plastic strain space. (ii) The 6D formulation implicitely asumes an influence of the hydrostatic pressure, which is wrong for materials with pressure insensitive yield functions. (iii) The mass moments of inertia are calculated with respect to a mean, which produces errors for certain load paths. (iv) Equation (6) gives wrong results for tension-torsion load paths, where it describes a circle in a σ versus $\sqrt{2}\tau$ diagram and not for the well known 90° phase shift with a circle in the σ versus $\sqrt{3}\tau$ diagram.

Hence, Meggiolaro and de Castro (2014) developed a different method. Therein, the stresses are represented in a 5D deviatoric stress subspace given by

$$\boldsymbol{\sigma}_{\text{dev}} = (S_1, S_2, S_3, S_4, S_5)^{\text{T}}, \tag{7}$$

where

$$S_1 = \sigma_{11} - \frac{\sigma_{22}+\sigma_{33}}{2}, \quad S_2 = \sqrt{3}\,\frac{\sigma_{22}-\sigma_{33}}{2}, \quad S_3 = \sqrt{3}\,\sigma_{12}, \quad S_4 = \sqrt{3}\,\sigma_{13}, \quad \text{and} \quad S_5 = \sqrt{3}\,\sigma_{23}. \tag{8}$$

By describing the stresses in the deviatoric stress space the aforementioned issues are solved due to the following reasons: It represents the plastic strain space, see (i), disregards the hydrostatic component, see (ii), and a circle in the σ versus $\sqrt{3}\tau$ diagram is recognized as such, see (iv). The moment of inertia matrix $\boldsymbol{I} \in R^5$ of the 5D stress path Σ is calculated independently of a mean, cf. (iii). It is given by the expression

$$\boldsymbol{I} = \frac{1}{L} \oint_{\Sigma} \boldsymbol{\sigma}_{\text{dev}}\, \boldsymbol{\sigma}_{\text{dev}}^{\text{T}}\, |\text{d}\boldsymbol{\sigma}|\,. \tag{9}$$

The non-proportionality factor f_{NP} is then calculated according to equation (6). This approach shows good agreement with experimental results for metals (Meggiolaro and de Castro, 2014). However, polymers, such as adhesive joints made of epoxy, are sensitive with respect to the hydrostatic pressure, see e. g. Beber et al. (2017); Adams (2005); Amos Gilat et al. (2005); Hu et al. (2003). That is accounted for in equation (4), but not in equation (9). However, the moment of inertia matrix should not be related to a mean, as already mentioned. We thus redefine

$$\boldsymbol{I} \in \mathbb{R}^6 = \oint_{\Sigma} \boldsymbol{\sigma}_M\, \boldsymbol{\sigma}_M^{\text{T}}\, |\text{d}\boldsymbol{\sigma}_M|\,. \tag{10}$$

In the latter expression, we combine the advantages of equation (4) and equation (9) by omitting the mean stress $\overline{\boldsymbol{\sigma}}$ and including the full stress tensor in Voigt notation in order to account for the hydrostatic pressure. Hence, the problem that a 90° phase shift path is not represented by a circle in the σ versus$\sqrt{3}\tau$ diagram still exists. However, we assume linear elastic material behavior of the adhesive when transforming load time series into stress time series as described in Noever Castelos and Balzani (2016b). A plastic strain path representation is thus not necessary. The non-proportionality factor f_{NP} is still computed following equation (6).

In order to compare the three approaches described above, 20 different synthetic stress paths are evaluated, see Figure 2. The choice of these paths is discussed in Itoh et al. (1995) and Meggiolaro and de Castro (2014). The characteristics of the underlying stress histories and the corresponding test case numbers are summarized in Table 1. The first 15 paths were taken

https://doi.org/10.5194/wes-2023-167
Preprint. Discussion started: 15 January 2024

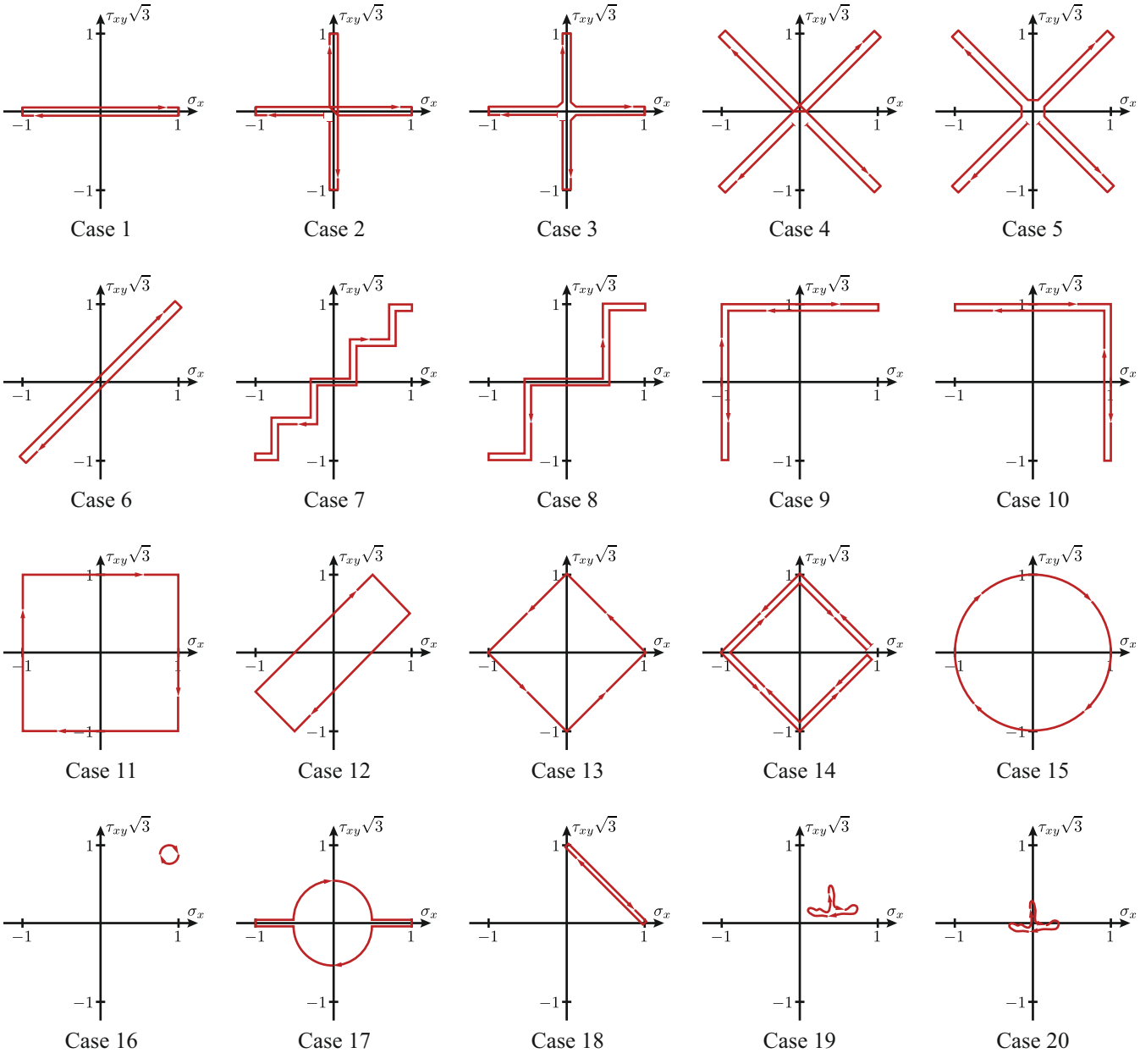

Figure 2. Load history test cases used for comparison of the non-proportionality factor approaches, extracted and reproduced from Itoh et al. (1995) and Meggiolaro and de Castro (2014).

from Itoh et al. (1995) and consider general factors like different or rotating principal stress directions, full reversed loadings or step length influences. From Meggiolaro and de Castro (2014), 5 additional critical paths were extracted, addressing e. g. a 90° phase shift or the influence of the mean stress.

https://doi.org/10.5194/wes-2023-167
Preprint. Discussion started: 15 January 2024

eawe european academy of wind energy
Open Access WIND ENERGY SCIENCE DISCUSSIONS

Table 1. Stress history characteristics of the applied 20 test cases. Test cases are taken from Itoh et al. (1995) and Meggiolaro and de Castro (2014) and are plotted in Figure 2.

Characteristics of stress histories	Text case number
Proportional loading	1,6
Only two principal stress directions	1-6
Full reversed loading	2-5
Rotating principal stress direction	2,6,9-15,17
Step length	6-10
90° phase shift	15
Small principal stress direction variation	7,16
45° principal stress direction variation	18
Mean value influence	9,10,16,18,19
Random path	19,20

Table 2 shows computational results of the f_{NP} test cases for the approaches according to Bishop (2000) and Meggiolaro and de Castro (2014) as well as the formulation proposed in this paper. These show that the derived method behaves in exactly the same way as the approach from Bishop (2000) for all load paths which are symmetric to the origin. Similar to Meggiolaro and de Castro (2014), it correctly predicts a nearly proportional stress path for test case 16 of $f_{NP} = 0.054$, where the formulation of Bishop (2000) recognises an ellipsis in the Voigt notation around a mean value and computes the same value as for test case 15 ($f_{NP} = 0.858$). This difference becomes also clear for the random loading centered in the origin (test case 20) compared to test case 19, where an offset was introduced. Test case 18 provokes the same problem for Bishop's approach (Bishop, 2000) considering the mean value but with the result that equation (4) only leads to one non-zero eigenvalue and thus to $f_{NP} = 0$, which represents proportional loading. However, this path is characterized by a 45° variation of the principal stress direction. For this stress path the method proposed in this work yields $f_{NP} = 0.555$, reflecting a similar value as the approach of Meggiolaro and de Castro (2014). In general, the non-proportionality factor proposed in this paper computes the same values for stress paths without mean values as Bishop's approach (Bishop, 2000) and tends to results of the formulation of Meggiolaro and de Castro (2014) for non-zero mean values. However, there is still some discrepancy to Meggiolaro's approach (Meggiolaro and de Castro, 2014) due to the different representation of the stress space.

3 Non-proportionality in trailing edge adhesive joints

The analysis of non-proportionality in fatigue stress histories for adhesive joints in wind turbine rotor blades is crucial for the understanding of the physical nature of fatigue damage and therefore for the choice of a reasonable method for the fatigue damage calculation. Therefore, three different blades are analysed in order to avoid blade-specific conclusions obtained from the study. Two rotor blades were chosen to compare similar-sized blades, one from the DTU 10 MW reference turbine (Bak

https://doi.org/10.5194/wes-2023-167
Preprint. Discussion started: 15 January 2024

eawe european academy of wind energy
Open Access WIND ENERGY SCIENCE DISCUSSIONS

Table 2. Comparison of the non-proportionality factors computed for the stress histories shown in Figure 2 according to Bishop (2000), Meggiolaro and de Castro (2014), and the approach proposed in this paper.

Test case	Bishop (2000)	Meggiolaro and de Castro (2014)	Proposed formulation
1	0.000	0.000	0.000
2	0.738	1.000	0.738
3	0.738	1.000	0.738
4	0.816	1.000	0.816
5	0.816	1.000	0.816
6	0.000	0.000	0.000
7	0.121	0.123	0.121
8	0.231	0.230	0.231
9	0.478	1.000	0.859
10	0.478	1.000	0.859
11	0.859	1.000	0.859
12	0.418	0.430	0.418
13	0.817	1.000	0.817
14	0.817	1.000	0.817
15	0.858	1.000	0.858
16	0.858	0.055	0.054
17	0.408	0.502	0.408
18	0.000	0.577	0.555
19	0.518	0.231	0.195
20	0.518	0.654	0.518

et al., 2013) with a length of 86 m, and the other one from the IWES IWT-7.5-164 reference turbine (Sevinc et al., 2016) with a length of 80 m. Additionally, the 20 m long pre-swept demonstrator blade (Bätge, 2016) from the *SmartBlades2* project (Tessmer et al., 2021), which is called *SB2-DemoBlade* in the following, is used to broaden the investigations to different blade sizes. Finite element (FE) models of the selected blades were generated with the in-house tool MoCA (Model Creation and Analysis tool), see Noever Castelos et al. (2022). Figure 3 shows the blade meshes of all three blades, highlighting the size differences. Ansys was used as the FE solver. The post-processing, i. e. the calculation and analysis of non-proportionality factors, was executed using own routines in Matlab.

All composite components of the blades are represented by 4-noded shell elements. The trailing edge adhesive joints are modelled with 8-noded solid elements, see the detail view in Figure 4 exemplarily for the IWES IWT-7.5-164 blade. Since the transitions from the root sections to the thin aerodynamic airfoils are different for the three blades (including the design of the trailing edge adhesive joints), the analyses are limited to the outboard regions of the blades at normalized radii of $0.45 < r/R < 0.9$, where r is the local radius, R is the rotor radius. Note that the radii are measured from the blade root, i.e.,

https://doi.org/10.5194/wes-2023-167
Preprint. Discussion started: 15 January 2024

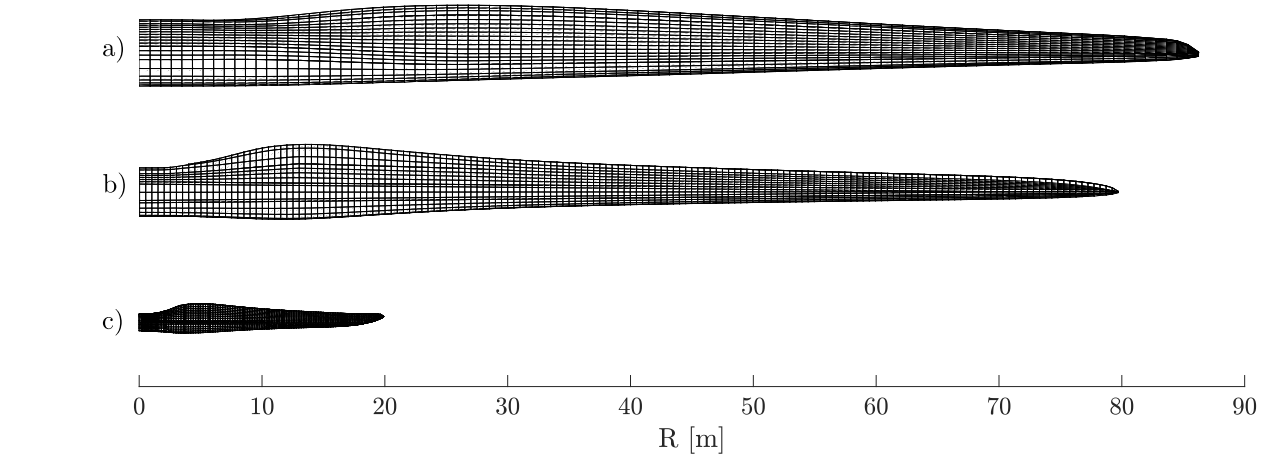

Figure 3. Finite element models of the three investigated rotor blades : a) DTU 10 MW (Bak et al., 2013), b) IWES IWT-7.5-164 (Sevinc et al., 2016), c) SB2-DemoBlade (Bätge, 2016)

the hub radius is neglected. The FE meshes are refined in the analysis regions in order to obtain better stress resolutions and stress convergence (local mesh refinement, not displayed in FE mesh images).

The non-proportionality of the adhesive joints is analysed on the basis of the fatigue load time series calculated for the design load case *power production* (DLC 1.2) according to the IEC standard 61400-1 Inernational Electrotechnical Commission (IEC) (2005). These load time series are translated to stress histories for each finite element representing the trailing edge adhesive joints according to the methodology described in Noever Castelos and Balzani (2016b). The non-proportionality factors f_{NP} are then calculated according to the newly proposed formulation introduced in section 2.

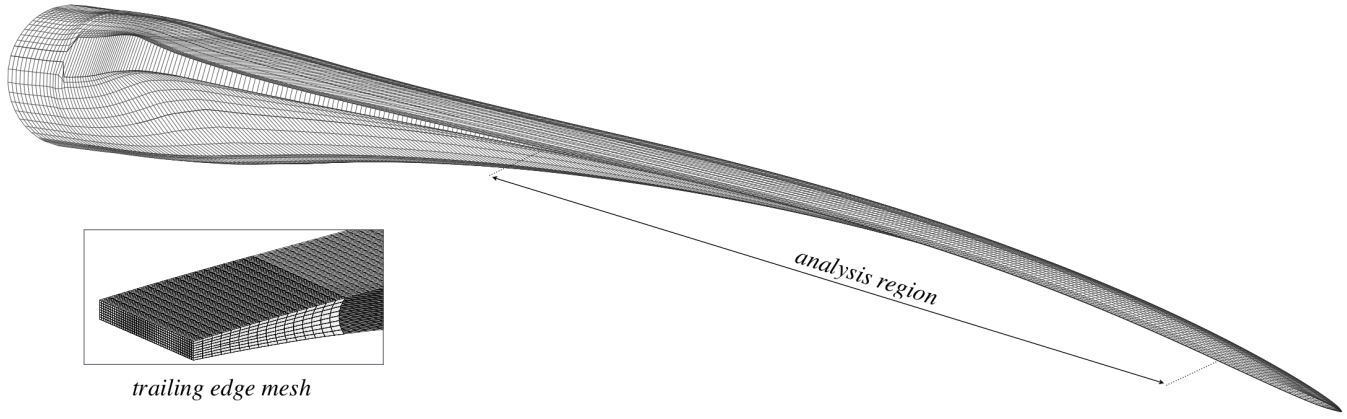

Figure 4. Visualization of the analysis region and a detailed view of the trailing edge FE mesh of the IWES-IWT-7.5 reference turbine blade.

https://doi.org/10.5194/wes-2023-167
Preprint. Discussion started: 15 January 2024

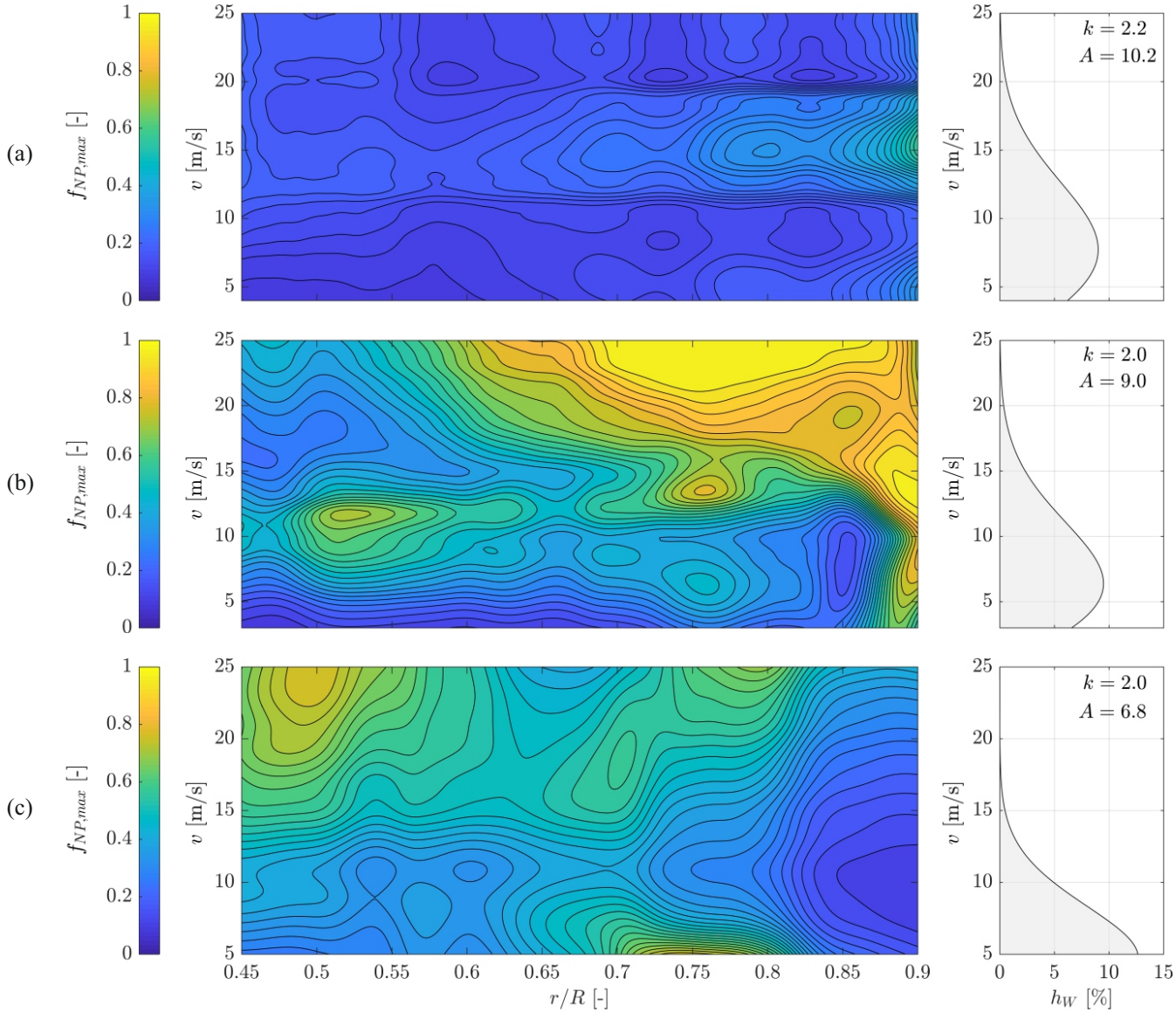

Figure 5. Contour plot of the non-proportionality factors as a function of the normalized radius r/R (on the x axis) and the wind velocity v (on the y axis): (a) DTU-10MW reference turbine blade (Bak et al., 2013); (b) IWES IWT-7.5-164 reference turbine blade (Sevinc et al., 2016); (c) SB2-DemoBlade (Bätge, 2016). Colour scale presented on the left, Weibull frequency of occurrence distribution of the wind velocity on the right.

In Figure 5, the maximum non-proportionality factors $f_{NP,max}$ found in the trailing edge adhesive elements in each cross-section along the span of the blade are illustrated as a contour plot for all three blades. Therein, the normalized radii r/R are

https://doi.org/10.5194/wes-2023-167
Preprint. Discussion started: 15 January 2024

eawe european academy of wind energy
Open Access WIND ENERGY SCIENCE DISCUSSIONS

plotted on the x axes and the wind velocities v on the y axes. The colour scale is given on the left, and the corresponding Weibull frequency of occurrence distributions of the wind velocities, h_W, on the right.

Figure 5 (a) depicts the results for the DTU 10 MW reference blade. A generally low degree of non-proportionality can be observed with a global average of about $f_{NP,max} = 0.2$. In a region close to the blade tip ($r/R > 0.85$), the local average reaches a maximum value of the non-proportionality factor of $f_{NP,max} = 0.4$ for wind speeds of $12 < v < 19$ m/s. When it comes to the contribution of fatigue damage (which is not evaluated in this paper), it is important to consider the frequency of occurrence of the wind velocity, as this will be used for the damage extrapolation in the assessment of the fatigue life. In the case of the DTU 10MW blade, an offshore Weibull distribution is used with a scaling factor of $A = 10.2$ m/s and a shape factor of $k = 2.2$. In this case, the wind velocities resulting in higher non-proportionality factors ($12 < v < 19$ m/s, see above), covers approximately 25 % of the year, whereas the lower wind velocities ($4 < v < 11$ m/s) appear in 64 % of the year, but result in much lower $f_{NP,max}$ values. However, the higher wind velocities are normally linked with higher stress amplitudes. The non-proportionality is thus considered to have a significant influence on the damage evolvement, at least in the regions where higher degrees of non-proportionality are present.

Although the IWES 7.5 MW blade is similar in length, the design is qualitatively very different to the DTU blade, see also Figure 3. The distribution of the non-proportionality factor along the span of the blade and the wind velocities hence also appears very much different. The degree of non-proportionality generally reaches much higher values than that in the DTU blade, see Figure 5 (b). In general, the degree on non-proportionality increases with the radius and the wind velocity. However, there is also a hot spot at a normalized radius of $0.5 < r/R < 0.55$ and a wind velocity of $9 < v < 12$ m/s and another one at $0.7 < r/R < 0.77$ and $13 < v < 16$ m/s. The Weibull frequency of occurrence distribution is one for a high wind speed near shore site (i.e., $A = 9.0$ m/s and $k = 2.0$). Hence, the high non-proportionality is present also at wind speeds with non-negligible probability.

The SB2-DemoBlade is much shorter than the other two blades. It is a pretty stiff blade design, but includes a pre-sweep for geometrical bend-twist coupling. The contour plot of the non-proportionality factor is shown in Figure 5 (c). The non-proportionality is generally higher than in the DTU blade, but not as high as in the IWES blade. Two hot spots are present at high wind velocities ($v > 18$ m/s) in two regions along the blade (i.e., $0.45 < r/R < 0.55$ and $0.73 < r/R < 0.82$). The site conditions for this blade design is low wind speed and onshore, hence $A = 6.8$ m/s and $k = 2.0$. The aforementioned Weibull parameters were derived from measurements of the field research validation site of NREL's CART3 turbine (Jager and Andreas, 1996) that the blade was designed for and set into operation for some time. Consequently, the wind velocity frequencies of occurrence are very low for the two non-proportionality hot spots. The non-proportionality may thus be irrelevant for the fatigue assessment. However, there is a third hot spot at a radial position of $0.68 < r/R < 0.8$ and a low wind speed of about 5 m/s. The frequency of occurrence of the wind speed in this location is very high, so the non-proportionality may affect the fatigue damage significantly here.

Figure 6 shows a representative excerpt (duration 50 s) of the stress time series in the trailing edge adhesive of all blades. A normalized radial position of $r/R = 0.77$ and the wind speed with the highest frequency of occurrence are chosen exemplarily. The stress time series are plotted for the element with the highest f_{NP} factor for the considered cross-sections and wind

https://doi.org/10.5194/wes-2023-167
Preprint. Discussion started: 15 January 2024

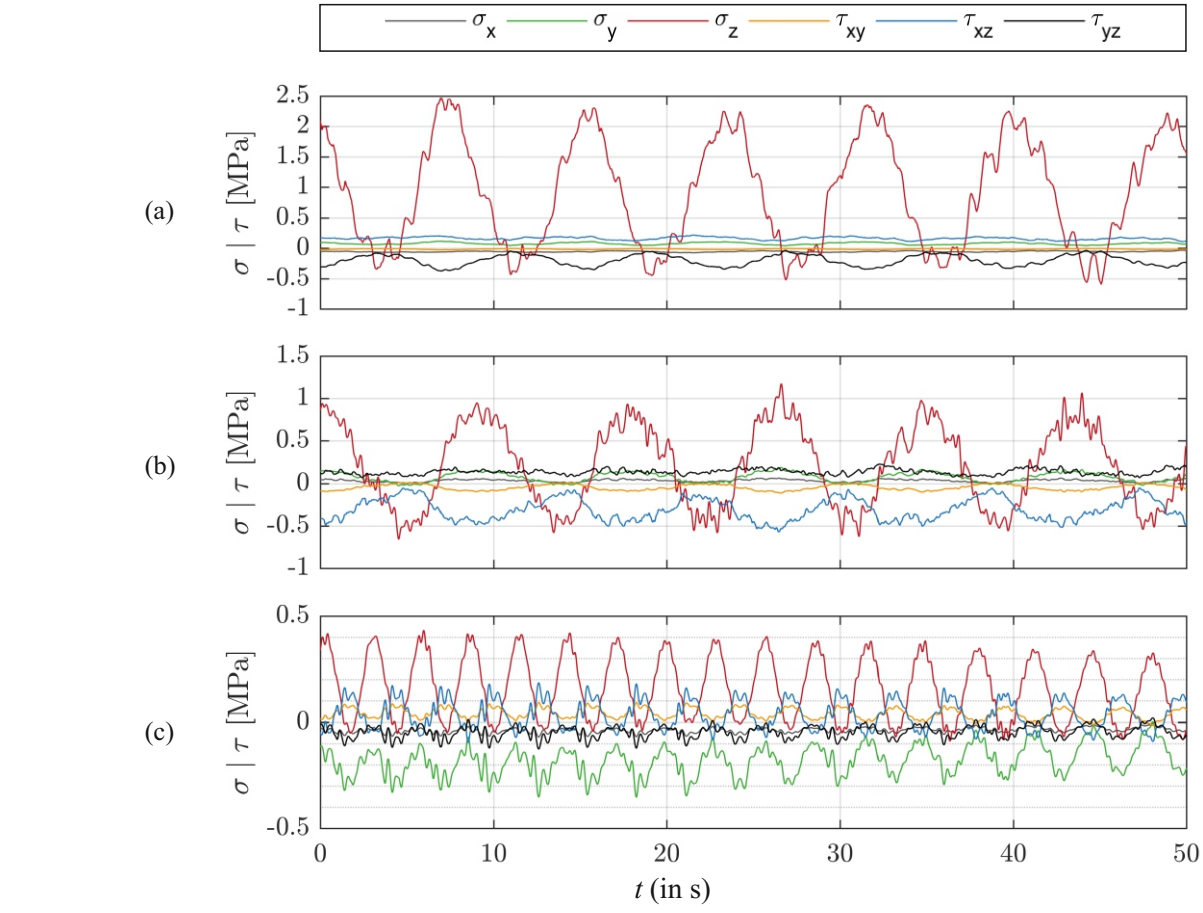

Figure 6. Stress histories of the finite element in the trailing edge adhesive joints with the highest non-proportionality at a normalized radial position of $r/R = 0.77$ for all investigated blades, related to the blade coordinate system according to DNV GL (2015): (a) DTU 10 MW reference blade, $v = 8$ m/s, $f_{NP} = 0.159$; (b) IWES IWT-7.5-164 reference blade, $v = 7$ m/s, $f_{NP} = 0.465$; (c) SB2 Demo blade, $v = 5$ m/s, $f_{NP} = 0.766$.

speeds. The stress results are calculated in the blade coordinate system according to DNV GL (2015), meaning that the z axis is pointing from the blade root to the blade tip, the y axis from the leading to the trailing edge, and the x axis from the pressure to the suction side. Hence, σ_x is the through-thickness normal stress in the adhesive, σ_y is the normal stress along the width of the adhesive, σ_z is the longitudinal normal stress, and τ_{xy}, τ_{xz}, and τ_{yz} are the in-plane and the transverse shear stresses, respectively.

The stress time series for the DTU blade is plotted in Figure 6 (a). It can be seen that the longitudinal stress σ_z is dominating the time series with an amplitude of approximately 1.5 MPa, a mean stress of approximately 1 MPa and a 1/revolution frequency. The mean stress is caused by the torque resulting in power output of the turbine. The oscillation is due to a high edgewise bending moment originating from the blade mass in rotation. The other stresses have negligible amplitudes and mean

https://doi.org/10.5194/wes-2023-167
Preprint. Discussion started: 15 January 2024

eawe european academy of wind energy
Open Access WIND ENERGY SCIENCE DISCUSSIONS

stresses. The dominating longitudinal normal stress corresponds to the small non-proporitonality factor of $f_{NP} = 0.159$ (i.e., almost proportional stress history) in the trailing edge adhesive displayed in Figure 5 (a), as this results in a very pronounced moment of inertia in the stress space in z direction and far smaller moments of inertia in the other dimensions.

Figure 6 (b) presents the stress time series for the IWES blade. The major excitation frequency is again 1per revolution and is of the same magnitude as that in the DTU blade, as the blade size is very similar. The longitudinal normal stress is still the dominant stress component. The amplitude is much lower compared to the DTU blade (approximately 0.75 MPa), as well as the mean stress (approximately 0.25 MPa). The reason is the different design philosophy expressed in the general blade shape (see Figure 3 resulting in a different mass distribution and a stiffer trailing edge girder reducing the strain and consequently the stress in the trailing edge adhesive. The through-thickness transverse shear stress τ_{xz} is remarkably higher than in the DTU blade, and also remarkably higher than all other stress components, but still significantly smaller than the longitudinal normal stress. However, it does contribute to the non-proportionality factor, especially since there is a 90° phase shift with respect to σ_z, see also test case 15 in section 2. Consequently, the non-proportionality factor is $f_{NP} = 0.465$, which is about three times higher than that in the DTU blade, see also Figure 5 (b).

The stress time series of the SB2-DemoBlade is presented in Figure 6 (c). It can be seen that the governing 1/revolution excitation frequency is much higher compared to the DTU and the IWES blades. This is due to the much smaller rotor diameter (tip speed ratio is a bit smaller, but the rotor diameter is about one fourth).The longitudinal normal stress σ_z has the highest amplitude of about 0.25 MPa and mean stress of approximately 0.15 MPa. In contrast to the DTU and the IWES blades, other stress components are much higher. E.g., the normal stress in width direction, σ_y, is about half as much as σ_z, which is not negligible. Moreover, the inplane and transverse shear stress in thickness direction, namely τ_{xy} and τ_{xz}, respectively, contribute notably with respect to amplitude. It is worth mentioning that the major part of the longitudinal normal stress is deterministic in nature, i.e., it shows a low amount of temporal variations from a sinusoidal signal. The other stress components have a much higher fluctuation, i.e., a higher stochastic content. The stress history for this blade results in a higher degree of non-proportionality expressed by a high non-proportionality factor at the exemplary location and wind speed of $f_{NP} = 0.766$. The reason for that is the higher contributions of stress components apart from the longitudinal stress. Some of these are in phase. E.g., the normal stresses σ_y and σ_z have the peaks and valleys at the same time. This normally results in a proportional stress history. However, the higher variability of σ_y contributes to non-proportionality. Other stress components, e.g., the shear stresses τ_{xy} and τ_{xz}, respectively, show a 90° phase shift to the aforementioned normal stresses, which naturally results in non-proportionality. The phase shift is due to the different excitation: The normal stresses σ_y and σ_z are governed by the blade mass in rotation, resulting in peaks and valleys when the blade is in 3 o'clock and 9 o'clock azimutal position. The shear stresses τ_{xy} and τ_{xz}, however, are influenced by asymmetries in the wind field, namely the wind shear, resulting in peaks and valleys at azimutal positions of 6 and 12 o'clock, respectively.

Up to here, the non-proportionality factor was given for each wind velocity. However, it is necessary to evaluate the degree of non-proporionality for the entire service life of the wind turbine including all possible wind velocities. A weighted mean value of the non-proporionality factor is thus calculated employing the wind velocity frequency of occurrence distribution function as a weighting factor. Introducing the cut-in and cut-out wind velocities by v_{in} and v_{out} and an integer number i identifying a

https://doi.org/10.5194/wes-2023-167
Preprint. Discussion started: 15 January 2024

eawe european academy of wind energy
Open Access WIND ENERGY SCIENCE DISCUSSIONS

wind speed bin, the weighted mean of the non-proportionality factor, $\bar{f}_{NP}$, is given by the relationship

$$\bar{f}_{NP} = \frac{\sum_{i=v_{\mathrm{in}}}^{v_{\mathrm{out}}} f_{NPi}\, h_{Wi}}{\sum_{i=v_{\mathrm{in}}}^{v_{\mathrm{out}}} h_{Wi}} \,. \tag{11}$$

Herein, f_{NPi} is the non-proporitonality factor for the given wind speed bin i and h_{Wi} is the frequency of occurence of said wind speed bin according to the Weibull distribution functions given in Figure 5.

Figure 7 shows $\bar{f}_{NP}$ distributed across the cross-section of the trailing edge adhesive joint at a radial position of $r/R = 0.77$ for all three blades, corresponding to the radial position of the stress history excerpt given in Figure 6. The cross-sectional views show a part of the suction side shells on the top and a part of the pressure side shells on the bottom. The trailing edge is on the right, respectively. As already concluded from the contour plots of Figure 5 and the stress histories in Figure 6, the DTU 10 MW blade shows the lowest and the SB2-DemoBlade the highest degree of non-proportionality. However, for all blades the distribution in the cross-section is qualitatively similar. The inner face of the adhesive joint has the highest degree of non-proportionality which is decreasing towards the trailing edge. This is due to the increasing distance to the principal bending axis and consequentially increasing longitudinal normal stresses σ_z from edge wise bending. The dominance of σ_z is thus increasing towards the trailing edge, making the stress histories more proportional.

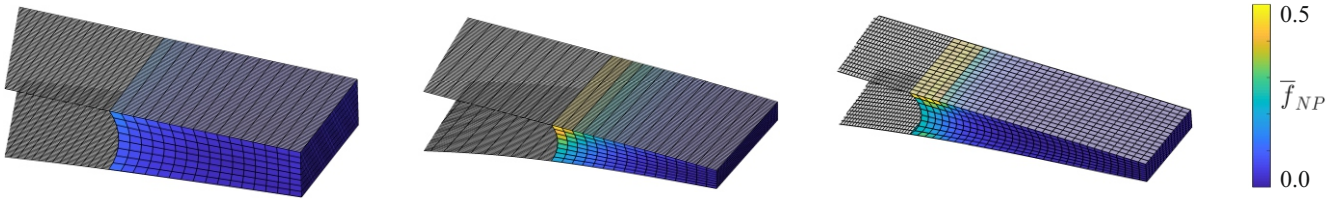

Figure 7. Contour plots of the weighted mean non-proportionality factor $\bar{f}_{NP}$ in the trailing edge adhesive for all three blades (cut-out with the visible cross-section at a radial position of $r/R = 0.77$) : (a) DTU blade; (b) IWES blade; (c) SB2-DemoBlade; (d) color code.

The maximum weighted mean non-proportionality factor in each cross-section, $\bar{f}_{NP,max}$, is plotted as a function of the normalized radial position for all three blades in Figure 8. In the DTU blade, the degree of non-proportionality factor is very low, see the explanations above. It is more or less constant at a value of $0.11 < \bar{f}_{NP,max} < 0.18$ along the blade, but increases towards the blade tip to its maximum of about 0.28. The IWES blade, which has a similar length, has moderate non-proportionality values of $0.3 < \bar{f}_{NP,max} < 0.4$ with a more distinct variability along the blade. The SB2-DemoBlade has a peak of non-proportionality at a radial position of $0.6 < r/R < 0.8$ with a maximum value of about 0.58. In this region, the non-proportionality factor is higher than in the other blades, whereas at smaller and larger radial positions, the degree of non-proportionality is lower than that in the IWES blade, and close to the tip also lower than that of the DTU blade. The large blades (DTU and IWES blade) behave somewhat similar close to the tip, where the degree of non-proportionality is increasing. Contrarily, the SB2-DemoBlade's non-proportionality is decreasing towards the blade tip. It can be seen that in general, the

https://doi.org/10.5194/wes-2023-167
Preprint. Discussion started: 15 January 2024

distribution of the maximum weighted mean non-proportionality factor along the blade is very different for the three blades analyzed in this work.

Generally, the non-proportionality degrees in the three blades are very different. It is thus difficult (or impossible) to draw general conclusions on the degree of non-proportionality with respect to blade size. Also, the higher degree of non-proportionality in the SB-DemoBlade could be triggered by the geometrical bend-twist coupling originated by the pre-sweep in the rotor area. We would like to emphasize that the DTU and IWES blades are numerical blade models that were developed for the research community. They may thus not be representative for a commercial blade designed for operation in the field. The SB2-DemoBlade, however, was designed for field testing of geometrical bend-twist coupling. The structural design was thus executed on a much higher level of detail, but due to the small size may not be representative for modern utility-scale wind turbines.

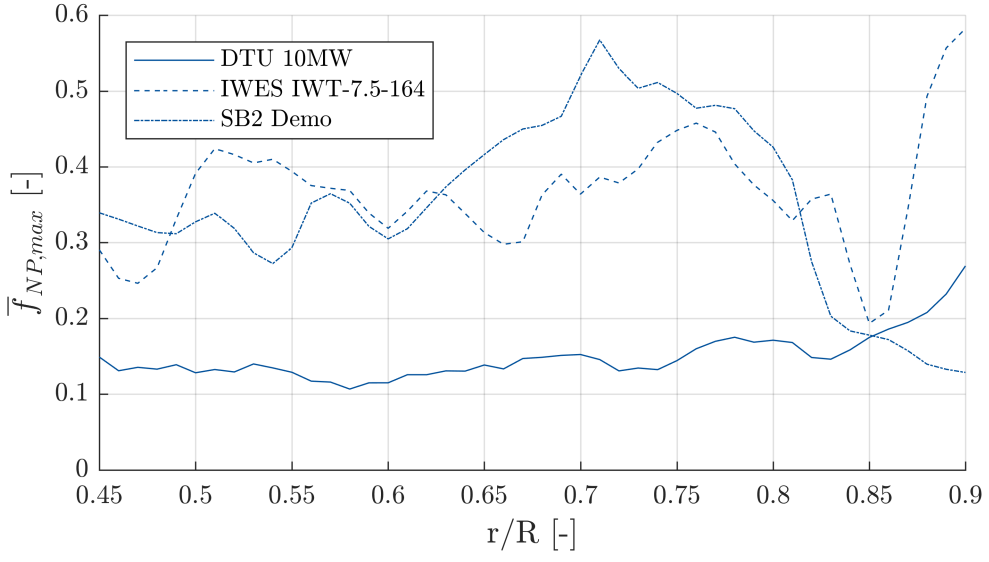

Figure 8. Maximum weighted mean non-proportionalty factor $\bar{f}_{NP,max}$ in the trailing edge adhesive joint plotted as a function of the normalized radial position r/R for all three blades.

4 Conclusions

In this paper, a non-proportionality factor was proposed that helps to quantify the degree of non-proportionality in a fatigue stress time series. Two different formulations from literature were combined. The non-proportionality factor was evaluated for 20 test cases on which the new formulation was benchmarked against other formulations. The agreement was excellent for those test cases where no difference was expected. It was further shown that the non-proportionality calculated with the new formulation is independent of a mean stress (which is an important feature) and accounts for hydrostatic pressure states. The

https://doi.org/10.5194/wes-2023-167
Preprint. Discussion started: 15 January 2024

new formulation is thus an improvement for materials that are sensitive to the presence of hydrostatic pressure in fatigue, as is the case for an epoxy-based adhesive investigated in this paper.

The non-proportionality factor was then applied to evaluate the degree of non-proportionality in trailing edge adhesive joints of three different rotor blades, two of which having a similar blade size and the third one being smaller and being equipped with a pre-sweep in the rotor plane. The characteristics of the degrees of non-proportionalities were analyzed in detail and were correlated with excerpts of the load time series.

The blade-specific design philosophies and the generally different mechanical responses prevent generalized conclusions on the degree of non-proportionality. However, it was shown that non-proportionality is generally present in each of the analysed blades. While it was very low in the DTU 10 MW blade, the degree of non-proportionality was significant in the IWES 7.5 MW blade and in the SB2-DemoBlade.

The distribution of the non-proportionality factor in the cross-section plane was similar in all cases and increased from the trailing edge towards the inner face corner on the suction side. It was observed that a dominating longitudinal normal stress, which can appear in real blades, reduces the degree of non-proportionality (which is also the reason for the cross-sectional distribution of the non-proportionality factor. If a blade is designed to have less dominant longitudinal normal stress, which may be a design goal to prevent tunneling cracks in the adhesive, the non-proportionality becomes more significant.

It was shown in literature that the choice of a suitable fatigue analysis framework depends on the degree of non-proportionality. For proportional stress histories, a global equivalent stress approach gives reasonable and accurate fatigue damage estimates. However, if there is a lot of non-proportionality involved, the critical plane approach needs to be utilized (which is computationally very intense), because the error of the global equivalent stress approach increases with the level of non-proportionality. Future work will thus have to clarify in how far the non-proportionality factor can be utilized as a decision-making metric in choosing an appropriate fatigue analysis procedure, finding the best compromise between accuracy and computational cost before actually carrying out the fatigue analysis.

Code and data availability. For legal reasons, code and data cannot be shared at this stage. The authors will try to provide code and data needed for reproduction of the findings by the time of final publication in case the manuscript will be accepted.

Author contributions. CB wrote the paper and provided scientific guidance and supervision to PNC in all project phases. PNC did the literature research, derived the equations, implemented pre- and postprocessing scripts in Matlab, carried out the simulations, prepared figures, and internally reviewed the manuscript.

Competing interests. The authors do not have competing interests.

https://doi.org/10.5194/wes-2023-167
Preprint. Discussion started: 15 January 2024

eawe european academy of wind energy
Open Access WIND ENERGY SCIENCE DISCUSSIONS

Disclaimer. The information in this paper is provided as is and no guarantee or warranty is given that the information is fit for any particular purpose. The user thereof uses the information at its sole risk and liability.

Acknowledgements. This research was funded by the Deutsche Forschungsgemeinschaft (DFG, German Research Foundation) as part of the Collaborative Research Center 1463 'Integrated Design and Operation Methodology for Offshore Megastructures' (SFB1463 – Project ID 434502799) and by the German Federal Ministry for Economic Affairs and Climate Actions (BMWK) of Germany as part of the coordinated research projects 'SmartBlades2' (Project ID 0324032C) and 'ReliaBlade' (Project ID 0324335B). The authors acknowledge the financial support.

https://doi.org/10.5194/wes-2023-167
Preprint. Discussion started: 15 January 2024

eawe european academy of wind energy
Open Access WIND ENERGY SCIENCE DISCUSSIONS

References

Adams, R. D.: Adhesive bonding: Science, technology and applications, CRC Press, Boca Raton, FL and Cambridge, 2005.

Amos Gilat, Robert K. Goldberg, and Gary D. Roberts: Strain Rate Sensitivity of Epoxy Resin in Tensile and Shear Loading, NASA, Springfield, 2005.

Anes, V., Reis, L., Li, B., and de Freitas, M.: New approach to evaluate non-proportionality in multiaxial loading conditions, Fatigue & Fracture of Engineering Materials & Structures, 37, 2014.

Antoniou, A. E., Vespermann, M. M., Sayer, F., and Krimmer, A.: Life prediction analysis of thick adhesive bond lines under variable amplitude fatigue loading, in: Proceedings of the 18th European Conference on Composite Materials (ECCM18), June 24-28, Athens, Greece, pp. 1–8, 2018.

Bak, C., Zahle, F., Bitsche, R., Kim, T., Yde, A., Henriksen, L. C., Natarajan, A., and Hansen, M. H.: Description of the DTU 10 MW Reference Wind Turbine, Tech. rep., DTU Wind Energy, 2013.

Bätge, M.: Design of a 20 m blade for the demonstration turbine (Deliverables 1.2.6.2/1.2.6.3), Schlussbericht Projekt SmartBlades, 2016.

Beber, V. C., Fernandes, P., Schneider, B., Brede, M., and Mayer, B.: Fatigue lifetime prediction of adhesively bonded joints: An investigation of the influence of material model and multiaxiality, International Journal of Adhesion and Adhesives, 78, 240–247, 2017.

Bishop, J. E.: Characterizing the non-proportional and out-of-phase extent of tensor paths, Fatigue & Fracture of Engineering Materials & Structures, 23, 1019–1103, 2000.

Christensen, R. M.: A two-property yield, failure (fracture) criterion for homogeneous, isotropic materials, Journal of Engineering Materials and Technology, 126, 45–52, 2004.

de Castro, J. T. P. and Meggiolaro, M. A.: Fatigue Design Techniques Under Real Service Loads, Volume II – Low-Cycle and Multiaxial Fatigue, CreateSpace Independent Publishing Platform, 1st edn., 2016.

Deng, Q.-Y., Zhu, S.-P., He, J.-C., Li, X.-K., and Carpinteri, A.: Multiaxial fatigue under variable amplitude loadings: review and solutions, International Journal of Structural Integrity, 13, 349–393, 2022.

Deng, Q.-Y., Zhu, S.-P., Niu, X., Lesiuk, G., Macek, W., and Wang, Q.: Load path sensitivity and multiaxial fatigue life prediction of metals under non-proportional loadings, International Journal of Fatigue, 166, 107 281, 2023.

DNV GL: DNVGL-ST-0376 – Rotor blades for wind turbines, 2015.

Downing, S. D. and Socie, D. F.: Simple rainflow counting algorithms, International Journal of Fatigue, 4, 31–40, 1982.

Drucker, D. C. and Prager, W.: Soil mechanics and plastic analysis or limit design, Quarterly of Applied Mathematics, 10, 157–165, 1952.

Eder, M. A., Semenov, S., and Sala, M.: Multiaxial Stress Based High Cycle Fatigue Model for Adhesive Joint Interfaces, in: Computational and Experimental Simulations in Engineering – Proceedings of ICCES2019, Mechanisms and Machine Science, vol 75, edited by Okada, H. and Atluri, S., pp. 621–632, Springer, Cham., 2020.

Endo, T., Mitsunaga, K., Takahashi, K., Kobayashi, K., and Matsuishi, M.: Damage evaluation of metals for random or varying loading – three aspects of rain flow method, Mechanical Behavior of Materials, 1, 371–380, 1974.

Fatemi, A. and Shamsaei, N.: Multiaxial fatigue: An overview and some approximation models for life estimation, International Journal of Fatigue, 33, 948–958, 2011.

Hu, Y., Xia, Z., and Ellyin, F.: Deformation behavior of an epoxy resin subject to multiaxial loadings. Part I: Experimental investigations, Polymer Engineering and Science, 43, 721–733, 2003.

Inernational Electrotechnical Commission (IEC): IEC Standard 61400-1, Wind turbines – Part 1: Design requirements, 2005.

https://doi.org/10.5194/wes-2023-167
Preprint. Discussion started: 15 January 2024

Itoh, T., Sakane, M., Ohnami, M., and Socie, D. F.: Nonproportional Low Cycle Fatigue Criterion for Type 304 Stainless Steel, Journal of Engineering Materials and Technology, 117, 285–292, 1995.

Itoh, T., Sakane, M., and Ohsuga, K.: Multiaxial low cycle fatigue life under non-proportional loading, International Journal of Pressure Vessels and Piping, 110, 50–56, 2013.

Jager, D. and Andreas, A.: NREL National Wind Technology Center (NWTC): M2 Tower; Boulder, Colorado (Data), 1996.

Kanazawa, K., Miller, K. J., and Brown, M. W.: Cyclic deformation of 1% Cr-Mo-V Steel under out-of-phase loads, Fatigue & Fracture of Engineering Materials & Structures, 2, 217–228, 1979.

Kuhn, M., Manousides, N., Antoniou, A., and Balzani, C.: Effects of non-proportionality and tension–compression asymmetry on the fatigue life prediction of equivalent stress criteria, Fatigue & Fracture of Engineering Materials & Structures, 46, 3161–3178, 2023.

Lee, Y.-L. and Tjhung, T.: Metal Fatigue Analysis Handbook – Practical problem-solving techniques for computer-aided engineering, chap. 3 – Rainflow Cycle Counting Techniques, pp. 89–114, Elsevier Inc., 2012.

Liu, X., Lu, C., Liang, S., Godbole, A., and Chen, Y.: Vibration-induced aerodynamic loads on large horizontal axis wind turbine blades, Applied Energy, 185, 1109–1119, 2017.

Manolas, D. I., Riziotis, V. A., and Voutsinas, S. G.: Assessing the Importance of Geometric Nonlinear Effects in the Prediction of Wind Turbine Blade Loads, Journal of Computational and Nonlinear Dynamics, 10, 041 008, 1–15, 2015.

Meggiolaro, M. A. and de Castro, J. T. P.: An improved multiaxial rainflow algorithm for non-proportional stress or strain histories – Part I: Enclosing surface methods, International Journal of Fatigue, 42, 217–226, 2012.

Meggiolaro, M. A. and de Castro, J. T. P.: Prediction of non-proportionality factors of multiaxial histories using the Moment Of Inertia method, International Journal of Fatigue, 61, 151–159, 2014.

Meggiolaro, M. A., de Castro, J. T. P., and Wu, H.: On the use of tensor paths to estimate the nonproportionality factor of multiaxial stress or strain histories under free-surface conditions, Acta Mechanica, 227, 3087–3100, 2016.

Noever Castelos, P. and Balzani, C.: On the impact of multi-axial stress states on trailing edge bondlines in wind turbine rotor blades, Journal of Physics: Conference Series, 753, 062 002, 2016a.

Noever Castelos, P. and Balzani, C.: The impact of geometric non-linearities on the fatigue analysis of trailing edge bond lines in wind turbine rotor blades, Journal of Physics: Conference Series, 749, 012 009, 2016b.

Noever Castelos, P., Haller, B., and Balzani, C.: Validation of a modeling methodology for wind turbine rotor blades based on a full-scale blade test, Wind Energy Science, 7, 105–127, 2022.

Raghava, R., Caddell, R. M., and Yeh, G. S. Y.: The macroscopic yield behaviour of polymers, Journal of Materials Science, 8, 225–232, 1973.

Rychlik, I.: A new definition of the rainflow cycle counting method, International Journal of Fatigue, 9, 119–121, 1987.

Schleicher, F.: Der Spannungszustand an der Fließgrenze (Plastizitätsbedingung), Journal of Applied Mathematics and Mechanics / Zeitschrift für Angewandte Mathematik und Mechanik (ZAMM), 6, 199–216, 1926.

Sevinc, A., Rosemeier, M., Bätge, M., Braun, R., Meng, F., Shan, M., Horte, D., Balzani, C., and Reuter, A.: Reference Wind Turbine IWT-7.5-164 Specification, Revision 2.0, Tech. rep., Fraunhofer Institute for Wind Energy Systems IWES, 2016.

Socie, D. F. and Marquis, G. B.: Multiaxial fatigue, Society of Automotive Engineers, Warrendale, Pa., 2000.

Stassi-D'Alia, F.: Flowand fracture of materials according to a new limiting conditionof yelding, Meccanica, 2, 178–195, 1967.

Stephens, R. I., Fatemi, A., Stephens, R. R., and Fuchs, H. O.: Metal fatigue in engineering, Wiley, New York, 2nd edn., 2001.

https://doi.org/10.5194/wes-2023-167
Preprint. Discussion started: 15 January 2024

Söker, H.: Advances in Wind Turbine Blade Design and Materials, chap. 2 – Loads on wind turbine blades, pp. 29–58, Woodhead Publishing Limited, Cambridge, UK, 2013.

Tessmer, J., Montano Rejas, Z. M., Rose, M., Daniele, E., Stoevesandt, B., Riemenschneider, J., Hölling, M., and Balzani, C.: SmartBlades2 – Bau, Test und Weiterentwicklung intelligenter Rotorblätter, Final Report (in German), 2021.

Teßmer, J., Icpinar, C., Sevinc, A., Daniele, E., Riemenschneider, J., Hölling, M., and Balzani, C.: Smart Blades – Entwicklung und Konstruktion intelligenter Rotorblätter, Final Report (in German), 2016.

van Kuik, G. and Peinke, J., eds.: Long-term Research Challenges in Wind Energy - A Research Agenda by the European Academy of Wind Energy, vol. 6 of *Research Topics in Wind Energy*, Springer International Publishing Switzerland, 2016.

van Kuik, G. A. M., Peinke, J., Nijssen, R., Lekou, D., Mann, J., Sørensen, J. N., Ferreira, C., van Wingerden, J. W., Schlipf, D., Gebraad, P., Polinder, H., Abrahamsen, A., van Bussel, G. J. W., Sørensen, J. D., Tavner, P., Bottasso, C. L., Muskulus, M., Matha, D., Lindeboom, H. J., Degraer, S., Kramer, O., Lehnhoff, S., Sonnenschein, M., Sørensen, P. E., Künneke, R. W., Morthorst, P. E., and Skytte, K.: Long-term research challenges in wind energy – a research agenda by the European Academy of Wind Energy, Wind Energy Science, 1, 1–39, 2016.

von Mises, R.: Mechanik der festen Körper im plastisch-deformablen Zustand, Nachrichten von der Gesellschaft der Wissenschaften zu Göttingen, Mathematisch-Physikalische Klasse, 4, 582–592, 1913.

Wentingmann, M., Noever Castelos, P., and Balzani, C.: An adaptive algorithm to accelerate the critical plane identification for multiaxial fatigue criteria, in: Proceedings of the 6th European Conference on Computational Mechanics: Solids, Structures and Coupled Problems and the 7th European Conference on Computational Fluid Dynamics (ECCM & ECFD 2018), edited by Owen, R., de Borst, R., Reese, J., and Pearce, C., pp. 3745–3754, CIMNE, Barcelona, Spain, 2018.

White, D. L. and Musial, W. D.: The Effect of Load Phase Angle on Wind Turbine Blade Fatigue Damage, Journal of Solar Energy Engineering, 126, 1050–1059, 2004.

Zouain, N., Mamiya, E. N., and Comes, F.: Using enclosing ellipsoids in multiaxial fatigue strength criteria, European Journal of Mechanics - A/Solids, 25, 51–71, 2006.